ELSEVIER

Polymer 44 (2003) 1771–1779

polymer

www.elsevier.com/locate/polymer

Molecular dynamics simulation of orientation and crystallization of polyethylene during uniaxial extension

Marc S. Lavine, Numan Waheed, Gregory C. Rutledge*

Department of Chemical Engineering, Massachusetts Institute of Technology, Cambridge, MA, 02139, USA

Received 28 September 2002; received in revised form 9 December 2002; accepted 9 December 2002

Abstract

Molecular dynamics simulations of realistic, united atom models of polyethylene undergoing uniaxial extension are described. Systems composed of chains ranging from 25 to 400 carbons have been studied, under a variety of processing histories, including isothermal deformation at constant applied stress below the melt temperature T_m, isothermal deformation below T_m followed by annealing, isothermal deformation above T_m followed by crystallization at a quench temperature below T_m, and non-isothermal crystallization during simultaneous deformation and cooling through T_m. Extension and orientation of large segments of flexible chains by uniaxial deformation accelerates the primary nucleation rate to a time scale accessible by molecular dynamics simulation. Entanglements operative during active deformation promote extension and orientation without nucleation of a crystal phase, while relaxation of stress at constant strain is sufficient to allow slippage of chains past pinning points and rapid nucleation and growth of crystallites as neighboring oriented chains come into registry. Isothermal crystallization of pre-oriented systems shows an apparent increase in nucleation density at lower temperatures; the resulting ordered regions are smaller and more closely aligned in the direction of orientation. During non-isothermal deformation, where stretching and cooling occur simultaneously, a first order transition is observed, with discontinuities in the volume and global order parameter, when the system crystallizes.

Keywords: Molecular dynamics; Crystallization; Nucleation

1. Introduction

The morphology of a semicrystalline polymeric material is prescribed by the crystalline form(s) (i.e. the unit cell), the crystalline habit (i.e. the shape and size of crystallites), the degree of crystallinity, and the orientation and spatial arrangement of the crystallites and intervening amorphous regions. Knowledge of morphology is central to understanding the overall mechanical properties exhibited by the material [1,2]. Considerable progress has been achieved in molecular level understanding of the structure and properties of the constituent crystalline [3–7] and inter-crystalline [8–10] regions through recent molecular simulations. Modeling of the detailed structure/property relationships in such dense systems requires retention of atomic level detail (for accurate prediction of crystallographic symmetry) or at the united atom level (for accurate description of structure at melt-like densities). In polymers, however, knowledge of equilibrium thermodynamic behavior alone appears to be insufficient to anticipate fully the several levels of structural organization that characterize a semicrystalline morphology. The semicrystalline state is a metastable one [11,12], the structure of which is dependent upon the kinetics of crystallization and the manner in which these kinetics give rise to a hierarchy of relevant length scales. Structures that equilibrate slowly relative to the crystallization time may be locked in during solidification, and can often be fortuitously manipulated through appropriate modification of processing conditions. Retaining the level of detail required to describe structure formation accurately, while at the same time accessing dynamical time scales where crystallization occurs, is a challenge for molecular simulation. Numerous efforts have been directed towards the study of *n*-alkane crystallization [13–17], crystallization of long chains in a structureless medium [18,19] or course-grained simulations using on-lattice kinetic Monte Carlo simulations with ad hoc moves [20–23]. Here,

* Corresponding author.
E-mail address: rutledge@mit.edu (G.C. Rutledge).

0032-3861/03/$ - see front matter © 2003 Elsevier Science Ltd. All rights reserved.
doi:10.1016/S0032-3861(03)00017-X

we retain a level of detail sufficient to identify with a particular chemical architecture (polyethylene) and use molecular dynamics to study the ordering processes that occur under the influence of applied deformation. Applied stress and deformation in the melt or solid state are exploited in the production of polymer fibers and films to enhance the crystallization rate, degree of crystallinity and to obtain morphologies with orientational order. The effects of orientation on crystallization are significant, and crystallization rates that are four or more orders of magnitude higher than those observed in the absence of orientation have been observed for polymers like poly(ethylene terephthalate) and polypropylene [24].

The role of deformation on crystallization has been rationalized in terms of enthalpic and entropic differences between deformed and undeformed melts. Both the enthalpy and entropy of a polymer melt are altered by the application of a large orienting deformation [25]. The enthalpy is lowered relative to the fully relaxed liquid through the improved packing of the chains, which reduces adjacent chain distances, and in some cases by the enhanced fraction of lower energy torsional states. The entropy is decreased through the reduction in the number of available chain conformations consistent with the oriented state. Peterlin [25] argued that the relative change in enthalpy will always be smaller than the change in entropy, so that the oriented melt is higher in free energy than the corresponding unoriented melt at the same temperature. Thus $T_{m\_oriented} \geq T_m$. The idea of melting point elevation has been used to explain the accelerated crystallization kinetics that are observed experimentally in fiber and film production. However, as demonstrated by Ziabicki and others ([26], and references therein), elevating T_m in the theoretical calculations is not sufficient to account for the four or five orders of magnitude increase in the crystallization kinetics observed experimentally. The crystalline morphology is also influenced by large orienting deformations. For polyethylene, the morphology changes from spherulitic to one dominated by long cylindrical crystallites or needles, surrounded by large epitaxial secondary growth, such as the shish-kebab morphology.

2. Method

All the simulations reported here were run using molecular dynamics methods as described by Allen and Tildesley [27]. We employ a united atom model where the hydrogen atoms are lumped onto the carbon atoms to which they are attached. We use the force field of Paul et al. [28], shown below and henceforth designated PYS

$$E_{BOND} = k_l(l - l_0)^2$$

$$E_{ANGLE} = k_\theta(\theta - \theta_0)^2$$

$$E_{TORSION} = k_0 + 1/2[k_1(1 - \cos(\varphi) + k_2(1 - \cos(2\varphi)) + k_3(1 - \cos(3\varphi))]$$

$$E_{vdW} = 4\varepsilon[(\sigma/r)^{12} - (\sigma/r)^6]$$

$k_1 = 350$ kcal/mol Å^{-2}, $l_0 = 1.53$ Å, $k_\theta = 60$ kcal/mol deg^{-2}, $\theta_0 = 109°$, $k_1 = 1.62$ kcal/mol, $k_2 = -0.86$ kcal/mol, $k_3 = 3.24$ kcal/mol, $\varepsilon = 0.112$ kcal/mol, $\sigma = 4.01$ Å. This force field was parameterized using experimental data and quantum calculations on short alkanes and has been shown to provide an accurate description of polyethylene melts [28–30]. The torsional term explicitly accounts for all intramolecular interactions between atoms separated by three bonds. Van der Waals interactions were truncated at 9 Å, and both pressure and energy were corrected for long range contributions assuming a homogeneous medium of density equal to that of the simulation cell. Periodic boundary conditions were used in all three dimensions. The choice of force field, in particular the stiffness of the torsional behavior, is a crucial factor in the study of crystallization in *n*-alkanes and polyethylene. A recent study [31] has confirmed the strong dependence of T_m and early stage crystallization kinetics on chain stiffness for a very simple chain model. Earlier studies [19,32] of atomically detailed chains have used the DREIDING force field [33] to characterize crystallization of polyethylene with molecular detail; this force field has almost no gauche well, and a cis barrier which is a factor of three too high, as shown in Fig. 1. It predicts a persistence length for polyethylene on the order of 50 Å [19], in contrast to the experimental value of 6 Å obtained by SANS [34] and the PYS force field [28]. Fig. 2 shows the configurations for two chains of length 500 carbons after 2 ns of simulation, each obtained in vacuum at 300 K after being allowed to collapse from a fully extended, all trans conformation, as was done in [19]. Fig. 2(a) shows a chain modeled by the DREIDING force field, while Fig. 2(b) shows a chain modeled by the PYS force field. The

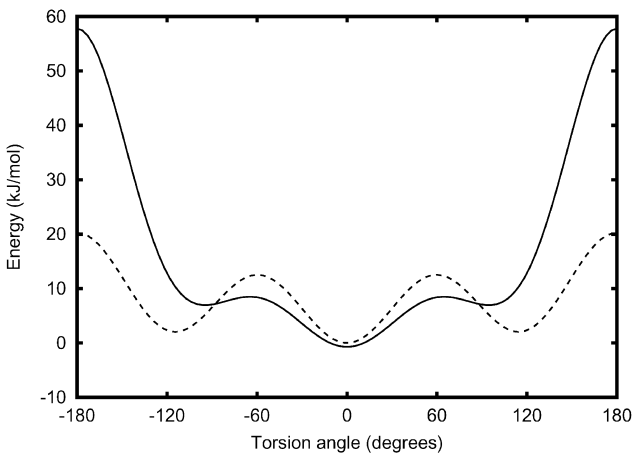

Fig. 1. Shapes of the torsional potential for two different polyethylene force fields used in earlier studies of polyethylene. Solid curve: DREIDING force field [33]; dashed curve: PYS force field [28].

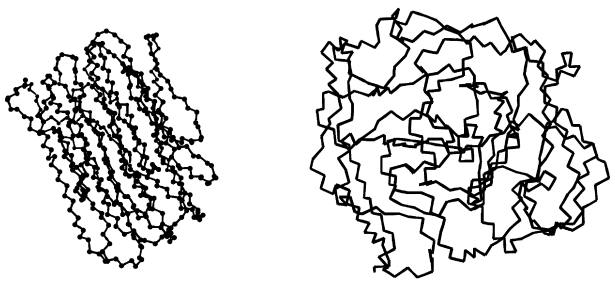

Fig. 2. Single chain of C500 in vacuum, simulated for 2 ns. The chain on the left was simulated following the work of Kavassalis and Sundararajan [19] using the DREIDING force field, and the one on the right using the force field of Paul et al. [28].

corresponding P_2 order parameters (see below) are 0.35 and 0.01, respectively. The stem length in the ordered regions of Fig. 2(a) is about 50 Å, considerably shorter than the 150 Å typically observed experimentally. Fig. 2(b) is more accurately characterized as a liquid drop on this time scale. Fig. 3 shows the corresponding torsion angle distributions for these two chains, averaged over 500 ps of simulation, with data taken every 10 ps; in the DREIDING force field, the fraction of gauche states is almost completely suppressed, while the *trans* state exhibits very broad shoulders. The recent Brownian dynamics simulations of Muthukumar and co-workers [18,35,36] use a similarly stiff torsional potential, which likely alters the dynamics of ordering as well. Here, instead of increasing chain stiffness to accelerate ordering, we take advantage of the documented increase in nucleation rates in deforming polymer melts, to study crystallization in realistic polyethylene chains under conditions relevant to high speed processing.

Simulations were performed in the NσT ensemble, with stress and temperature regulated using the method of Berendsen [37]. The thermostat control T_T was set between 0.2 and 5.0 ps, similar to the range of values evaluated by Berendsen. This results in deviations of 5 K or less from the

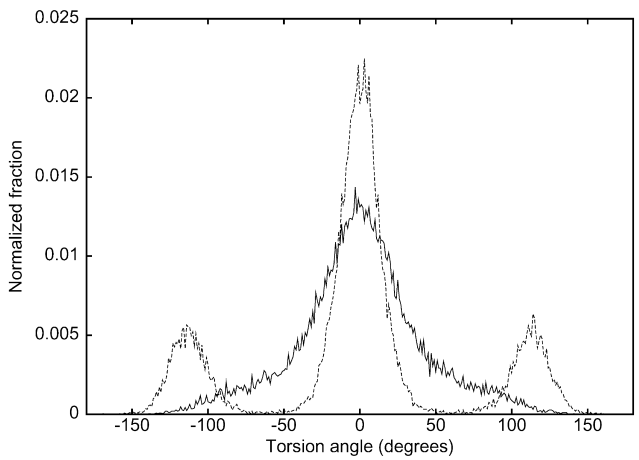

Fig. 3. Torsional distribution for the chains shown in Fig. 2, averaged over the last 500 ps of simulation, with data taken every 10 ps. DREIDING force field (solid line); PYS force field (dashed line).

set point, in the absence of a phase transition. Smaller deviations were observed for smaller values of T_T. No noticeable difference in the crystallization behavior was observed for values of T_T within this range. The barostat control T_P was typically set to a value between 300 and 3500 ps, similar to the range of values (relative to the range of stresses applied) tested by Berendsen. In this work, we have increased both T_P and the applied stresses ($\sigma_{xx} \sim 10^8$ Pa) used during simulation; the higher values for T_P help to suppress unacceptably large changes in box shape that would result in unphysical overlap of atoms between successive steps of simulation. Two approaches were used to re-scale the size and/or shape of the cell during a simulation. For all simulations involving extensional deformation (i.e. with an external applied stress $\sigma_{xx} > 0$) and for most of the relaxation studies (i.e. $\sigma_{xx} = \sigma_{yy} = \sigma_{zz} = 0$ following a simulated extensional deformation), the scaling factors were determined independently for each of the three directions, namely $\lambda_x \neq \lambda_y \neq \lambda_z$; the simulation cell could undergo significant changes in both volume and shape. For some of the relaxation studies, a single factor λ was used for scaling all three directions, thereby allowing the volume to change, but preventing a change in the overall shape. We found that this protocol precludes the elastic recoil typically observed in the stretching direction upon cessation of deformation; only slow densification is observed during relaxation. In all simulations, the cell retained orthorhombic symmetry, and $\sigma_{yy} = \sigma_{zz} = 0$.

The equations of motion were integrated using the velocity Verlet method with an integration time step (Δt) that ranged from 1 to 5 fs. The larger time step leads to a systematic drift in potential energy, primarily in the bond stretching component, which is mitigated by use of the thermostat. To ensure that none of the crucial structural quantities were affected, we compared simulations of melts of chains 400 carbons long (C400, NPT and NVT ensembles, 5 chains at 1 atm, 450 K, 1 ns duration) using 1 and 5 fs time steps. On average, the bond lengths in the simulation with $\Delta t = 5$ fs were 10% longer than those in the simulation with $\Delta t = 1$ fs, leading to a 20% increase in bond energy. In all metrics of relevance to monitoring crystallization (i.e. trans fraction, sequences of trans torsions, and orientational order parameters), the differences between the two simulations were negligible ($<2\%$ deviation).

We also compared simulations of deforming melts (5 chains of C400 at 300 K) using $\sigma_{xx} = 1 \times 10^8$ Pa and $\sigma_{xx} = 2 \times 10^8$ Pa, and $\Delta t = 1$, 3 and 5 fs. Here too, the bond contribution to potential energy equilibrated at a higher value for longer time steps, but no significant difference was observed in structural quantities. The larger time step appears to enhance the diffusion rate of the chains and to decrease slightly the likelihood of a chain segment residing in a torsional state close to that of the minimum energy. These two effects oppose each other, with the consequence that no detectable difference in crystallization kinetics was observed for simulations with time steps between 1 and 5 fs.

The development of order and crystallinity was monitored through metrics based on torsion angle values and orientational order parameters. Orientational order parameters were found to be particularly useful indicators of crystal formation in a companion study of crystal growth of *n*-eicosane, yielding results comparable to, but more sensitive than, a density-based order parameter [17]. The unit vector characterizing the local chain direction at each atom was computed from the chord connecting second neighbor atoms: $\mathbf{e}_i = (\mathbf{r}_{i+1} - \mathbf{r}_{i-1})/|\mathbf{r}_{i+1} - \mathbf{r}_{i-1}|$. Parallel alignment of chains was then computed as follows (where i and j index different atoms)

$$P_2 = \tfrac{3}{2}\langle(\mathbf{e}_i \cdot \mathbf{e}_j)^2\rangle - \tfrac{1}{2}. \quad (1)$$

Similarly, alignment of chain segments with the applied stress direction was monitored using

$$P_{2X} = \tfrac{3}{2}\langle(\mathbf{e}_i \cdot \mathbf{e}_x)^2\rangle - \tfrac{1}{2} \quad (2)$$

where $\mathbf{e}_x$ is the unit vector in the direction of applied stress, σ_{xx}.

Lastly, we monitored the formation of crystallizable sequences of length 1–5 bonds long. Since polyethylene crystallizes in the all-*trans* conformation, the fractions of conformers of length $n = 1$–5 in the all-*trans* state, i.e. $p_{\text{trans}}(n)$ were calculated. For these calculations, the *trans* state was defined to include torsion angles lying between −60 and +60°. Visual inspection of individual configurations and of trajectories was performed using Xmol 1.31 [38].

3. Results and discussion

3.1. Influence of chain length

A large deformation was applied to a set of moderate to long alkane chains, ranging from 25 to 400 carbons in length (henceforth denoted C*n*, where *n* is the carbon number). These chain lengths were chosen to cover a range of molecular weights from well below the entanglement length for polyethylene, which has been estimated to be 150 backbone carbons [39], to well above it. Fig. 4 shows the strain as a function of time for four different chain lengths subjected to a constant applied stress (NσT ensemble) at 300 K. For the C25 chains, the cell dimensions deform rapidly, as there is little resistance to reorientation of the molecules. For the C200 and C400 chains, the strain responses are similar and relatively insensitive to molecular weight. This is indicative of chains above the entanglement molecular weight, where the response is determined by the entanglement length rather than the chain length; we expect still longer chains to behave similarly. For intermediate chain lengths such as the C100 system, the initial response is comparable to that of the longer chains (strain rate ca. $7 \times 10^9\ \text{s}^{-1}$), but deviates to larger strains on the time scale

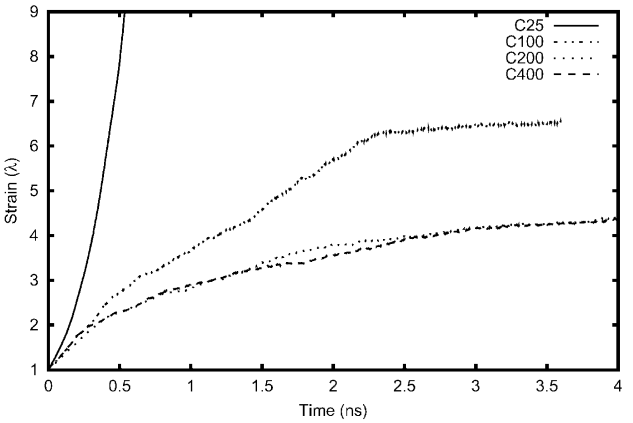

Fig. 4. For a constant applied stress ($\sigma_{xx} = 1.5 \times 10^8$ Pa), the strain is shown as function of time for systems with four different chain lengths. The number of chains is varied to maintain a total of 2000 atoms in the simulation cell in each case.

of 1–3 ns, in accord with a characteristic relaxation time, τ_{Rouse}, of 2 ns for the end-to-end vector of C100 [30,40]. Fig. 5 shows the chain slip response for several chains whose configurations were extracted from simulation of the C100 system, at intervals of several nanoseconds. Each chain resolves into 3 or 4 segments, separated by 'pinning points', which deform rapidly and orient along the deformation direction. 'Entangled' behavior apparently requires 6–8 such pinning points per chain. Disengagement of a particular chain from its pinning points can be identified by rapid changes in the radius of gyration of the chain (R_g). This is shown in Fig. 6 for the four representative chains singled out for illustration in Fig. 5. Neither chain 7 nor chain 11 show any sudden changes in its R_g. In the former case, the chain was not pinned by its neighbors, and thus shows a continuous increase in R_g until the chain approaches full extension. In the latter case, the chain is unable to escape its pinning points, and thus shows only minimal increase in R_g. Both chain 2 and chain 9 are examples of chains that show sudden changes in R_g due to liberation of a pinning point. For chain 2, this leads to a sudden increase in

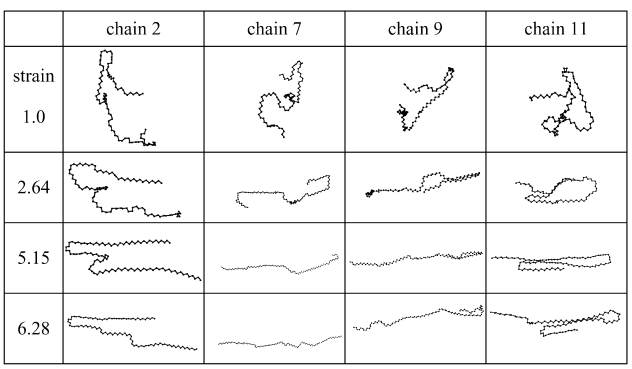

Fig. 5. Conformations of four representative chains of C100, illustrated at different stages of deformation. The localization of kinks in the chains, with long, extended segments in between, are interpreted as being due to entanglements (see text for details).

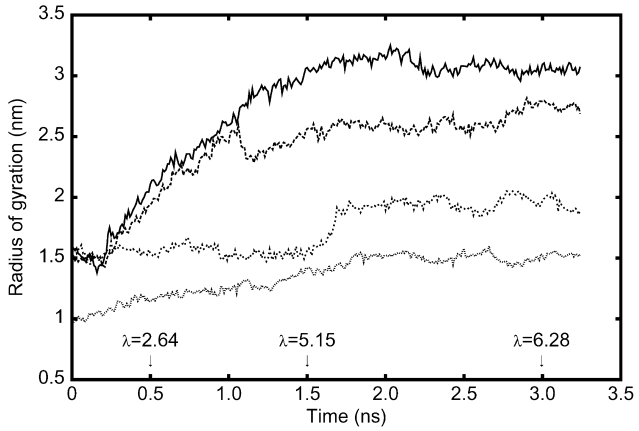

Fig. 6. Radius of gyration versus time for the four representative chains shown in Fig. 5: from top to bottom: chain 7; chain 9; chain 2; chain 11.

R_g and then a plateau, as no further freeing of pinning points occurs. For chain 9, there is a sudden decrease in R_g, which then increases as the chain approaches full extension (except for a partial fold back at one end). This apparently anomolous behavior is due to the fact that the initial response of the chain to the liberated pinning point is lateral contraction, followed by subsequent elongation.

3.2. Extensional deformation below T_m

For the system consisting of 20 chains of C100, a series of simulations was performed with the applied stress σ_{xx} ranging from 1×10^8 to 4×10^8 Pa at 300 K. A series of snapshots from a typical deformation of the C100 system at 1.5×10^8 Pa is shown in Fig. 7. Starting from an initial slab, the cell rapidly deforms under the applied stress, with the x-dimension of the cell roughly doubling in the first 500 ps ($\lambda = 2.64$). Following this initial rapid deformation, the rate of strain is much slower, doubling the x-dimension of the cell again only after 1500 ps ($\lambda = 5.15$). Beyond this point, the cell deforms very slowly as the simulation proceeds, and one can observe large sections of fully extended chain segments.

The development of orientational order and alignment suggested by Fig. 7 can be described quantitatively using the global order parameters, P_2 and P_{2x}. These are shown in Fig. 8 for several different applied stresses. As shown in Fig. 8(a), an initial linear increase in P_2 with strain is followed, above a threshold strain, by a weaker dependence of P_2 on strain. The value of threshold strain (λ_{crit}) decreases with increasing applied stress. The deformation behavior can be compared to the deformation behavior of a glassy polymer that is assumed to undergo pseudo-affine deformation with respect to the strain dependence of P_{2X} [41]. In that case, the reorientation of bond chords should scale with strain as $\tan(\theta')/\tan(\theta) = \lambda^{1.5}$ where θ' and θ are the angles that the new and old bond chord make with the direction of the applied stress. Fig. 8(b) shows the dependence of P_{2X}

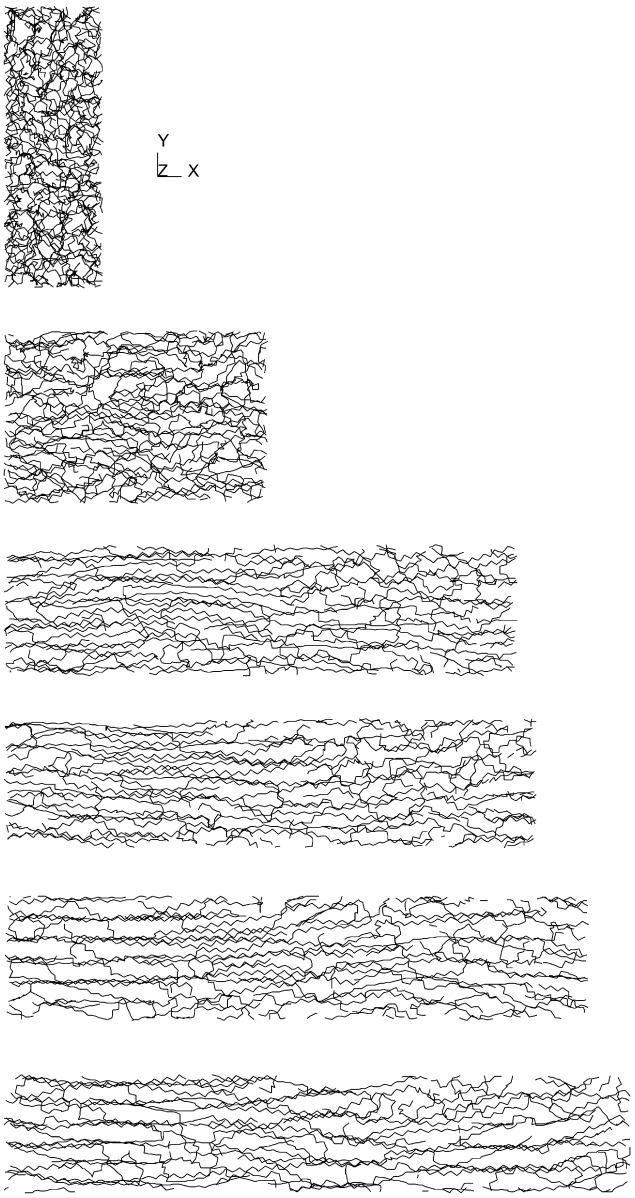

Fig. 7. Snapshots of a system of 20 C100 chains, deformed at 300 K (same as Fig. 4). From top to bottom: $\lambda = 1.00$ (initial box); $\lambda = 2.64$; $\lambda = 5.15$; $\lambda = 5.34$; $\lambda = 5.86$; $\lambda = 6.28$. The initial box dimensions are $1.88 \times 5.32 \times 5.32$ nm and the final box dimensions are $11.8 \times 2.23 \times 1.96$ nm.

versus λ for the same C100 simulations. Also shown is the expected behavior according to pseudo-affine deformation. The latter appears to be a good description of deformation at low strain, but deviates in all cases for $\lambda > 1.5$; this deviation from pseudo-affine behavior is independent of, and precedes, λ_{crit} which occurs at values of λ between 3 and 4. Simulations performed above 400 K, close to the melt temperature, do not exhibit pseudo-affine behavior, even at low strain. This indicates that deformation is homogeneous only at low strain and well below T_m; at longer times and higher temperatures, conformational relaxation is significant and behavior is non-glassy.

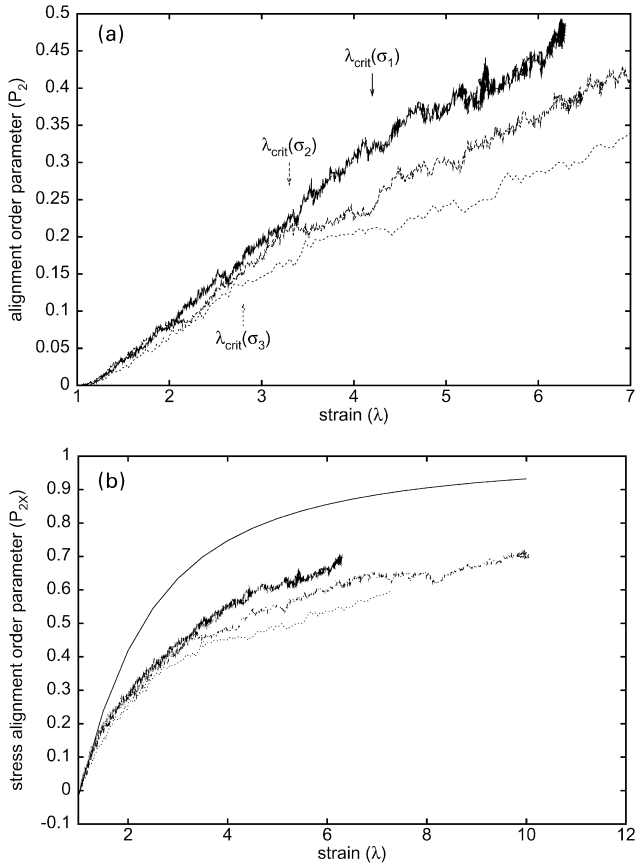

Fig. 8. (a) Development of parallel alignment order (P_2) as a function of strain (λ) for 20 C100 chains deformed under uniaxial elongation at 300 K: $\sigma_{xx} = 1.5 \times 10^8$ Pa (solid line); $\sigma_{xx} = 2.0 \times 10^8$ Pa (dashed line); $\sigma_{xx} = 4.0 \times 10^8$ Pa (dotted line); The corresponding threshold strains are 4.2, 3.3 and 2.8, for $\sigma_{xx} = 1.5 \times 10^8$, 2.0×10^8 and 4.0×10^8 Pa, respectively. (b) Development of alignment order in the stress direction (P_{2X}) as a function of strain (λ) for the same systems as (a). The solid curve is the pseudo-affine deformation response.

3.3. Isothermal deformation and crystallization

In the last two frames of Fig. 7 it is possible to observe regions that appear to be crystalline, as characterized by both intramolecular conformation order (i.e. fully extended chain segments) and intermolecular packing order. Thus it would appear that a nucleation event might have occurred in this simulation. However, *continued active deformation* of the cell from this point did not result in growth of this nucleus. In order to study the nucleation and growth of the crystalline phase, we repeated the simulation of extensional deformation with a system containing five C400 chains under an applied stress of $\sigma_{xx} = 1.5 \times 10^8$ Pa at 300 K, allowing both volume and shape of the simulation cell to vary. This pre-oriented system was then allowed to evolve at zero applied stress for a period of 12 ns at 300 K, under conditions of variable volume but fixed shape, i.e. with a single λ. Fig. 9 shows snapshots of the system, illustrating clearly the nucleation and growth of ordered regions in the simulation cell. The top image is representative of the

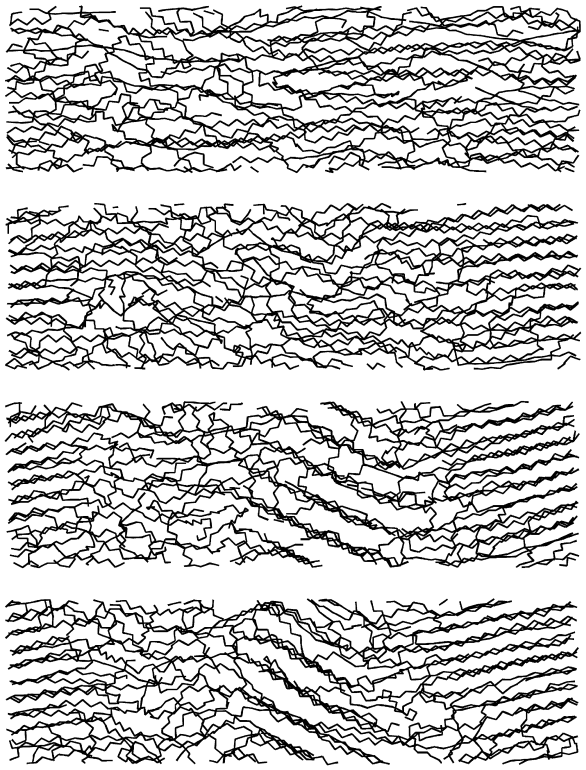

Fig. 9. Snapshots of a system of five C400 chains at 0, 4, 8 and 12 ns of evolution after deformation at 300 K (from top to bottom). The volume was allowed to change during the relaxation, subject to the constraint that all dimensions are scaled by a single scaling factor (see text for details).

system at the end of the deformation stage, while the bottom image is taken after 12 ps of annealing. In the top image, one can see small regions where the chain segments are fully extended and aligned with segments of neighboring chains. As before, continued active deformation did not induce significant crystallinity. However, upon transition from active deformation to annealing, the chains reorganize, allowing nascient nuclei to grow rapidly, resulting in measurable crystallinity within the simulation. This simulation illustrates the importance of molecular mobility and relaxation to the development of nuclei and crystalline-like order. The constrained shape of the simulation precludes the possibility that this is a simple consequence of elastic recoil. Rather, nucleation occurs through local rearrangement of aligned molecular segments.

Further study of nucleation and growth was limited by the small size of the simulation cell in this case. Once formed, the ordered region quickly attains a size comparable to the smallest dimension of the simulation cell and is stabilized by the periodic boundary conditions. Further deformation results in void formation. To avoid this limitation, we increased the system size to 8000 atoms and repeated simulations under conditions of isothermal elongation followed by annealing. Fig. 10 shows snapshots taken from a set of simulations which were prepared by stretching twenty C400 chains at 425 K and $\sigma_{xx} = 1 \times 10^8$ Pa and then subsequently quenching them

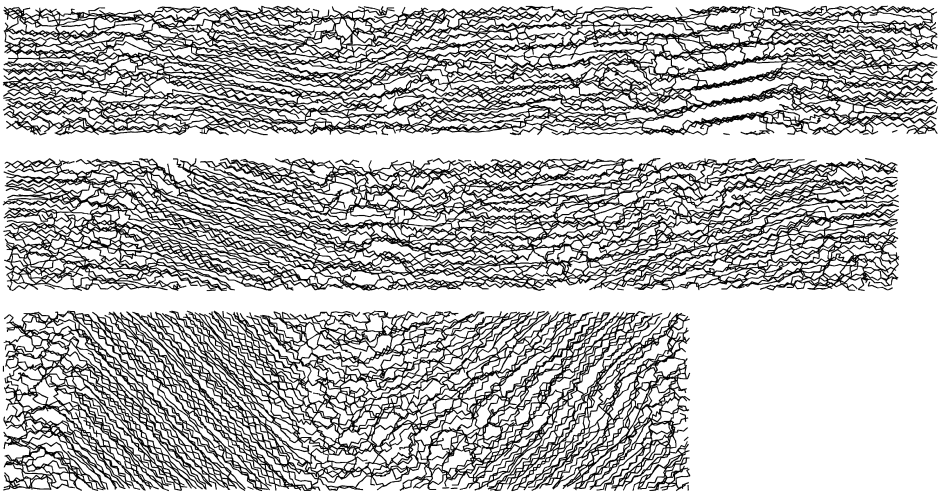

Fig. 10. Snapshots of a system of twenty C400 chains which was initially deformed at 425 K and then quenched to 250, 300 and 350 K (from top to bottom) and allowed to evolve. At each temperature, the shapshots were taken after the systems showed an initial plateau in the alignment order parameter (P_2), corresponding to $t = 5.5$, 9.5 and 18.0 ns, respectively.

to 250, 300 or 350 K. In this set of simulations, orientation develops under an applied stress during the simulation above T_m, where mobility is high and nucleation does not occur; hence there is less risk of void formation during active deformation and larger strains are possible. Stress is then removed and the temperature quenched to below T_m, where nucleation and growth occur. Box shape was not fixed in this instance. The orientation developed under an applied stress significantly reduces the barrier to nucleation, while the annealing period plays an important role in allowing chains to come into registry and crystallize. The snapshots in Fig. 10 were taken when plateaus were first observed in the P_2 and P_{2X} data; these corresponded to P_2 values of 0.6, 0.4 and 0.15 and P_{2X} values of 0.7, 0.5 and 0.25, observed at times of 5.5, 9.5 and 18.0 ns of isothermal crystallization, for 250, 300 and 350 K, respectively. At the lowest crystallization temperature (250 K), the system showed a rapid increase in order and decrease in volume. From Fig. 10, one can see a large number of small regions with well ordered chains that are closely aligned with the applied stress direction, separated by poorly oriented regions, indicative of small crystallites or nascent nuclei. At the highest crystallization temperature (350 K), the order developed much more slowly, and there was greater retraction of the chains in the stretching direction. Much fewer but larger crystals form at this temperature.

The increase in nucleation rate at the expense of crystal growth at larger supercooling is well known from crystallization experiments and theory [22]. As can be seen in Fig. 10, in addition to differences in the number of crystals and their sizes, the angle that the crystal c-axis makes with the stress direction increases as the annealing temperature increases. Both these results are in agreement with recent work by Blundell and co-workers [42–46], who report similar observations in studies of crystallization of poly (ethylene terephthalate) during application of an elongational stress, as well as subsequent to release of this stress. This can be interpreted as a competition between two kinetic processes, the rate of relaxation of deformation-induced orientation and the rate of nucleation which locks in structure at some level of orientation.

3.4. Non-isothermal deformation and crystallization

We also performed simulations under conditions of non-isothermal elongation, in which most of the strain and associated orientation develops while the system is above T_m. Non-isothermal elongation is most similar to the conditions that occur in a fiber production line. A system of five C400 chains was stretched with $\sigma_{xx} = 1 \times 10^8$ Pa, and $\Delta t = 2$ fs, starting at a temperature 450 K and cooled to 250 K over a period of 20 ns. Fig. 11 shows the changes in volume and order parameter as a function of temperature. Between 360 and 320 K rapid densification takes place,

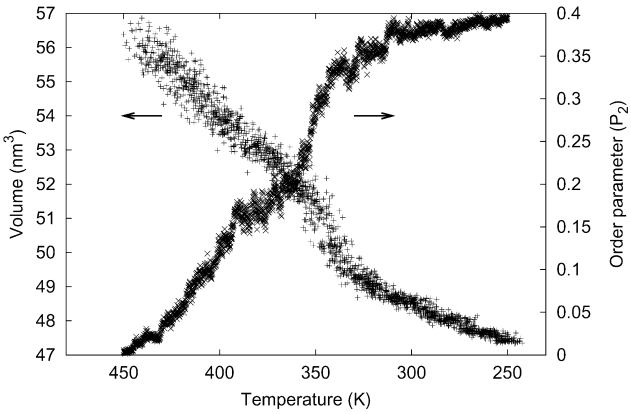

Fig. 11. For a simultaneous cooling and stretching simulation, the volume (+) and global alignment order parameter P_2(×) are plotted as a function of temperature. At approximately 360 K, the order parameter shows a sharp transition, which is matched by a volume decrease characteristic of a material undergoing crystallization.

accompanied by a corresponding increase in the order parameter, indicative of crystallization. Below 340 K, the slope of the volume–temperature curve continues to decrease, as more of the system is converted from melt to crystal phase. The order parameter curve has a second important feature, showing a change in slope at a temperature of 390–380 K, which is just below the melt temperature for polyethylene. This plateau region corresponds to a temperature range where there is a balance between the loss of thermal energy, which encourages crystallization, and the work of deformation, which continually destroys small, nascient nuclei. From visual images of the chain configurations shown in Fig. 12, one can see a small nucleus that forms at around 380 K (corresponding to 7 ns). With continuing strain the nuclei is unstable and melts, until it reforms at 360 K and then grows into a larger crystal, as shown in Fig. 12. This is in agreement with crystal melting observed during the two stage biaxial stretching of a polymer films, where the crystals that form during the initial draw phase are subsequently melted by the second drawing stage in the orthogonal direction.

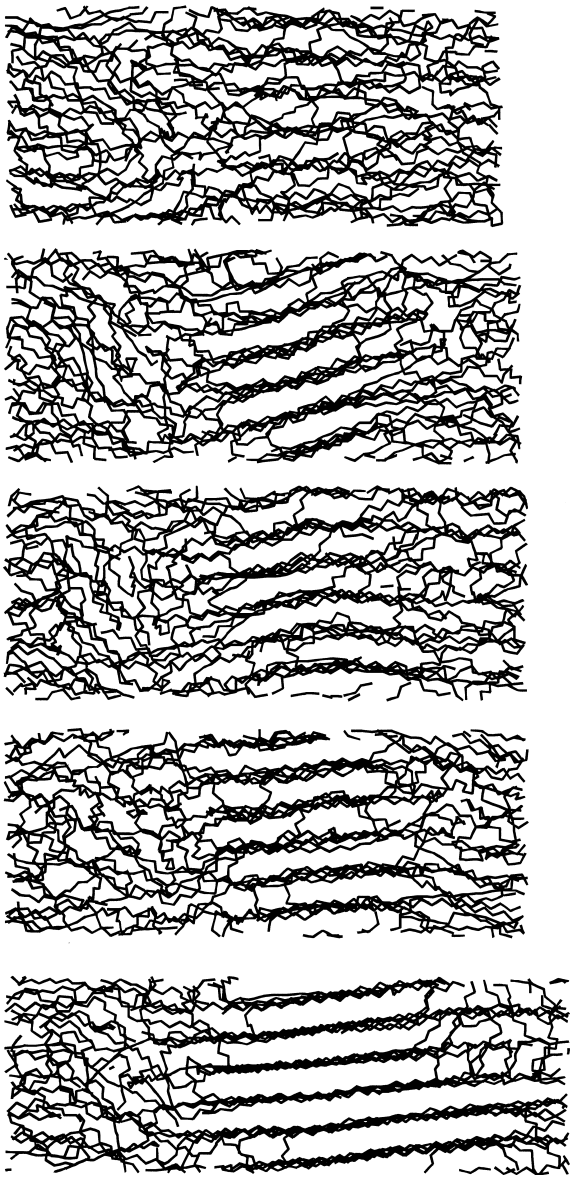

Fig. 12. Chain configurations from a non-isothermal deformation simulation. From top to bottom, the images were taken at 374, 368, 364, 360 and 290 K, corresponding to 7.6, 8.2, 8.6, 9.0 and 16.0 ns.

4. Conclusions

Extension and ordering of melts ranging from *n*-alkanes (C25) to entangled polyethylene (carbon number >150) can be observed by direct simulation under conditions of applied uniaxial stress. The addition of a large deforming stress accelerates the crystallization process by driving chains into the lower energy trans torsional conformation and by aligning long *trans* sequences in a single direction. In the absence of such imposed extension and orientation, the primary nucleation rate for crystallites of realistic, flexible chains in the melt is too slow to observe readily by direct simulation with currently available workstations. Extension and orientation of large segments of the chains reduce the barrier to primary nucleation, allowing observation of such events on the time scale accessible to molecular dynamics simulation.

Under conditions of uniaxial deformation, crystallization is a function of both total strain and strain rate. A sufficient total strain is required to extend the polyethylene chains and align the chain segments parallel to each other. At the high strain rates typical of molecular dynamics simulation and at temperatures below T_m, crystallization is partially suppressed, as entangled chains can become tightly bound at local pinning points. Active pinning points prevent the molecules from sliding past each other, a degree of freedom which is apparently necessary for the formation of nuclei. However, above a threshold strain, sufficient extension and orientation develops to allow rapid nucleation as soon as deformation is stopped.

Below T_m pseudo-affine deformation is observed at low strains. Above T_m pseudo-affine deformation is not observed, even at relatively low strains and high strain rates. When deformation and cooling are applied in conjunction, a clear first-order crystallization transition is observed, as measured by changes in the volume and global order parameter, and confirmed by direct visualization.

Acknowledgements

We would like to thank Drs Jonathan Harris and Sandeep Patel for making their molecular dynamics source code available to us. Financial support for this work was provided by the ERC Program of the National Science Foundation under Award Number EEC-9731680, the Center for Advanced Engineering Fibers and Films.

References

[1] Lin L, Argon AS. J Mater Sci 1994;29(2):294–323.
[2] Al-Hussein M, Davies GR, Ward IM. J Polym Sci B 2000;38(5): 755–64.
[3] Sorensen RA, Liao WB, Kesner L, Boyd RH. Macromolecules 1988; 21(1):200–8.
[4] Tashiro K. Prog Polym Sci 1993;18(3):377–435.
[5] Lacks DJ, Rutledge GC. J Phys Chem 1994;98(4):1222–31.
[6] Martonak R, Paul W, Binder K. Phys Rev E 1998;57(2):2425–37.
[7] Rutledge GC, Lacks DJ, Martonak R, Binder K. J Chem Phys 1998; 108(24):10274–80.
[8] Balijepalli S, Rutledge GC. J Chem Phys 1998;109(16):6523–6.
[9] Balijepalli S, Rutledge GC. Comput Theor Polym Sci 2000;10(1–2): 103–13.
[10] Gautam S, Balijepalli S, Rutledge GC. Macromolecules 2000;33(24): 9136–45.
[11] Strobl GR. The physics of polymers, 2nd ed. Berlin: Springer; 1997.
[12] Hu W, Albrecht T, Strobl G. Macromolecules 1999;32(22):7548–54.
[13] Yamamoto T. J Chem Phys 1997;107(7):2653–63.
[14] Yamamoto T. J Chem Phys 1998;109(11):4638–45.
[15] Takeuchi H. J Chem Phys 1998;109(13):5614–21.
[16] Esselink K, Hilbers PAJ, Beest BWHV. J Chem Phys 1994;101(10): 9033–41.
[17] Waheed N, Lavine MS, Rutledge GC. J Chem Phys 2002;116(5): 2301–9.
[18] Liu C, Muthukumar M. J Chem Phys 1998;109(6):2536–42.
[19] Kavassalis TA, Sundararajan PR. Macromolecules 1993;26(16): 4144–50.
[20] Goldbeck-Wood G. In: Dosière M, editor. Crystallization of polymers. Netherlands: Kluwer Academic Publisher; 1993. p. 249–55.
[21] Chen C-M, Higgs PG. J Chem Phys 1998;108(10):4305–14.
[22] Armistead K, Goldbeck-Wood G. Adv Polym Sci 1992;100:219–312.
[23] Doye JPK, Frenkel D. J Chem Phys 1998;109(22):10033–41.
[24] Shimizu J, Okui N, Kikutani T. In: Ziabicki A, Kawai H, editors. High-speed fiber spinning: science and engineering aspects. New York: Wiley; 1985. p. 429–83; Chapter 15.
[25] Peterlin A. In: Miller RL, editor. Flow-induced crytallization in polymer systems. New York: Gordon and Breach Science Publishers; 1979. p. 1–29.
[26] Ziabicki A. Fundamentals of fibre formation. London: Wiley; 1975.
[27] Allen MP, Tildesley DJ. Computer simulation of liquids. Oxford: Clarendon Press; 1987.
[28] Paul W, Yoon DY, Smith GD. J Chem Phys 1995;103(4):1702–9.
[29] Mavrantzas VG, Theodorou DN. Macromolecules 1998;31(18): 6310–32.
[30] Harmandaris VA, Mavrantzas VG, Theodorou DN. Macromolecules 1998;31(22):7934–43.
[31] Miura T, Kishi R, Makami MYT. Phys Rev E 2001;63:061807.
[32] Fujiwara S, Sato T. Phys Rev Lett 1998;80(5):991–4.
[33] Mayo SL, Olafson BD, Goddard III WA. J Phys Chem 1990;94(26): 8897–909.
[34] Horton JC, Squires GL, Boothroyd AT, Fetters LJ, Rennie RJ, Glinka CJ, Robinson RA. Macromolecules 1989;22(2):681–6.
[35] Muthukumar M, Welch P. Polymer 2000;41(25):8833.
[36] Welch P, Muthukumar M. Phys Rev Lett 2001;87:218302.
[37] Berendsen HJC, Postma JPM, van Gunsteren WF, DiNola A, Haak JR. J Chem Phys 1984;81(8):3684–90.
[38] X Mol. NetworkCS; 1993.
[39] Kremer K, Grest GS. J Chem Phys 1990;92(8):5057–86.
[40] Paul W, Smith GD, Yoon DY. Macromolecules 1997;30(25): 7772–80.
[41] Ward IM, Hadley DW. An introduction to the mechanical properties of solid polymers. New York: Wiley; 1993.
[42] Blundell DJ, MacKerron DH, Fuller W, Mahendrasingam A, Martin C, Oldman RJ, Rule RJ, Riekel C. Polymer 1996;37(15):3303–11.
[43] Blundell DJ, Mahendrasingam A, Martin C, Fuller W, MacKerron DH, Harvie JL, Oldman RJ, Riekel C. Polymer 2000;41(21): 7793–802.
[44] Mahendrasingam A, Martin C, Fuller W, Blundell DJ, Oldman RJ, Harvie JL, MacKerron DH, Riekel C, Engström P. Polymer 1999; 40(20):5553–65.
[45] Mahendrasingam A, Martin C, Fuller W, Blundell DJ, Oldman RJ, MacKerron DH, Harvie JL, Riekel C. Polymer 2000;41(3):1217–21.
[46] Mahendrasingam A, Blundell DJ, Martin C, Fuller W, MacKerron DH, Harvie JL, Oldman RJ, Riekel C. Polymer 2000;41(21): 7803–14.